Energy Dependence of Electron Damage in Copper*

A. SOSIN
Research Division, Atomics International, Division of North American Aviation, Inc., Canoga Park, California
(Received October 23, 1961, revised manuscript received February 12, 1962)

Electron irradiation below 1-Mev and subsequent recovery in copper have been investigated. The minimum threshold displacement energy is found to be less than 22 ev. The details of the recovery in stage I, as a function of electron energy, are found to be more complex than anticipated. Specifically, I_a decreases, I_b increases slowly, and I_c increases rapidly, respectively, in relative importance as the electron energy is reduced. A calculation of the cross section for displacement of copper atoms by electrons is also presented. A Born-Mayer potential with standard parameters is used. Only displacements in or near the close-packed directions are evaluated in detail. Other directions do not appear to contribute significantly in the near threshold energy region being considered. The agreement between this theory and experiment is found when a minimum threshold displacement energy between 19 and 20 ev and a Frenkel resistivity between 2 and 3 μohm cm per atomic percent of interstitial-vacancy pairs is assumed.

INTRODUCTION

THE recovery of electrical resistivity of copper on annealing in stage I (<65°K) following radiation damage has been studied intensively in recent years. Following the initial demonstration of Cooper, Koehler, and Marx[1] of the existence of stage I after deuteron irradiation, Magnuson, Palmer, and Koehler[2] resolved four substages, again following deuteron irradiation. Corbett, Smith, and Walker,[3] studying recovery after 1.4-Mev electron irradiations, have resolved five substages and measured the activation energies for annealing in each substage, designated as I_a, I_b, I_c, I_d, and I_e in order of increasing temperature at which they occur. Furthermore, Corbett *et al.* found the three lower temperature substages, with activation energies of 0.05, 0.085, and 0.095 ev, respectively, to obey first-order kinetics, thereby suggesting the recombination of close interstitial-vacancy pairs; this interpretation was reinforced by the determination of a reaction rate constant commensurate with a single atomic jump. Corbett *et al.* also showed that substages I_d and I_e possess the same activation energy, 0.12 ev, and, based on other considerations as well, suggested that I_d represents correlated recombination of interstitials and vacancies, while I_e represents uncorrelated recombination of interstitials and vacancies during long-range interstitial migration. A model limited to this description would, in a perfect crystal, require complete annihilation of all interstitials and vacancies, created in equal number by electron irradiation. Corbett *et al.* have suggested that interstitials can combine with other interstitials, predominantly forming dimers (clusters of two interstitials), which are immobile in Stage I_e and that the cross section for dimer formation is approximately equal to that for pair recombination.

Subsequently, Meechan, Sosin, and Brinkman[4] reported that the amount of resistivity recovery in stage I, following electron irradiation, typically between 85 and 90%, can be altered if the sample is rather heavily deformed (at room temperature) prior to irradiation. Thus 29% area reduction reduced stage I recovery to 76%, 91% area reduction, to 71%. They further showed that the additional resistivity which is retained in deformed samples is entirely recovered in stage III (~300°K); in fact, superrecovery may occur—the resistivity recovers to a level below its pre-irradiation value.

Blewitt *et al.*[5] have investigated stage I recovery following fast-neutron irradiation. No simple picture emerges from these data—less recovery is observed, substage structure cannot be easily resolved, and recovery is found to begin at temperatures below the range of substage I_a. It was shown that the presence of impurities inhibits recovery in stage I.

All of these experiments, as well as many other related ones, have sought to provide a basis for a unique interpretation of defect migration and association in metals. Nevertheless, no completely acceptable model has evolved as yet. Two factors have been investigated in this study. First, the rate of resistivity increase as a function of electron energy has been studied. Second, the dependence of the character of the annealing in stage I on the energy of incident electrons has been examined. Actually, some results on energy dependence have already been reported by Corbett and Walker[6] and by Chaplin and Shearin.[7] The present work extends down to lower energies. In this way, it has been possible to approach the minimum threshold energy for atomic displacements, as well as to observe the considerable importance of electron energy on the subsequent recovery spectrum.

* Research supported by the U. S. Atomic Energy Commission.

[1] H. G. Cooper, J. S. Koehler, and J. W. Marx, Phys. Rev. **97**, 599 (1955).

[2] G. D. Magnuson, W. Palmer, and J. S. Koehler, Phys. Rev. **109**, 1990 (1958).

[3] J. W. Corbett, R. B. Smith, and R. M. Walker, Phys. Rev. **114**, 1452 (1959); Phys. Rev. **114**, 1460 (1959).

[4] C. J. Meechan, A. Sosin, and J. A. Brinkman, Phys. Rev. **120**, 411 (1960).

[5] T. H. Blewitt, R. R. Coltman, C. E. Klabunde, and T. S. Noggle, J. Appl. Phys. **28**, 639 (1957).

[6] J. W. Corbett and R. M. Walker, Phys. Rev. **115**, 67 (1959).

[7] R. L. Chaplin and P. E. Shearin, Phys. Rev. **124**, 1061 (1961).

EXPERIMENTAL DETAILS

The cryostat which has been used in this work has been described elsewhere.[8] The features of this cryostat which are important here are the following:

(1) The samples are irradiated directly by the electron beam. There are no intervening foils, etc., thereby eliminating the need for an appropriate energy correction.

(2) The samples are cooled by conduction to a reservoir maintained at 4.2°K during irradiation and measurement. Calculations and measurements indicate that the (typically) 5 μa/cm^2 beam used produced maximum heating of less than 2°K, at any incident electron energy. This is also true for heating in the samples (0.0053 cm diam, 1.3 cm long) due to the (typically) 200-ma measuring current.

(3) A mechanical valve for liquid helium and a fine manganin heater allow sharp temperature pulses to any temperature below about 100°K; typically, the rise time to elevated temperature is about 20 sec with less than five sec spent in traversing the last two-deg interval. Cooling to 4.2°K is essentially instantaneous. Since the duration of the usual isochronal pulse at temperature is 5 min, no time correction has been made.

(4) Between irradiation, the sample is warmed to over 350°K in place, thereby annealing nearly all the previous damage.

(5) Thermometry is provided by a Cu vs Au-3.2% Co alloy, kindly supplied by Corbett and Walker. This couple emf was compared with a platinum resistance thermometer and with the temperature dependence of electrical resistivity of copper. The calibration which has been used probably is not better than ± 0.5°K in the range between 4.2° and 100°K.

The pure copper samples were fabricated from bar stock (99.999% stated purity) provided by American Smelting and Refining Company. The stock was wire drawn through diamond dies to the final diameter and annealed to vacuum to 450°C for about one hour after mounting on a sample holder, fully described elsewhere.[8] The measured residual resistivity ρ_0 of the sample was about 5×10^{-9} ohm cm.

Resistance measurements are made using a Rubicon Thermofree microvolt potentiometer. The current is controlled, using a circuit due to Garwin,[9] to about one part in 10^5. The precision of measurement is about $\pm 2\times10^{-12}$ ohm cm.

The electron energy is the quantity subject to the largest error. Although Van de Graaff accelerators are basically stable, the observed energy oscillation and limits of energy resolution indicate an energy uncertainty of ± 15 kev. Furthermore, the accelerator, nominally a 2-Mev Van de Graaff generator, was calibrated at one point using the Be(γ,n) nuclear reaction at 1.655 Mev. Since this energy calibration point is not within the range of electron energies used in this present work, it is possible that the final error may be somewhat larger.

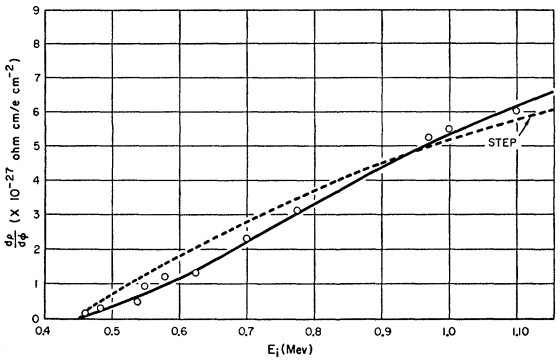

FIG. 1. The dependence of damage rate $d\rho/d\phi$, the resistivity increase per integrated electron flux, on incident electron energy. The data points are circled.

The precision in integrated flux is best appreciated by referring to the full description of the apparatus.[8] The design of the equipment includes an efficient Faraday cage for determining the total integrated flux. Evidence for the relative accuracy of the arrangement is demonstrated by the precision with which the resistivity was observed to increase linearly with dose. On occasion, two samples of pure copper have been mounted in the cryostat (which normally accommodates four samples). This sort of experiment indicates that the absolute damage rate at a fixed electron energy is subject to more sizable error, estimated at about 5%. Presumably, this is due to an inhomogeneity in the electron density in the beam. Since the beam is observed to shift position in time, the linearity of the resistivity increase vs dose curves depends on the persistence of the operator in maintaining fixed beam conditions by use of the various adjustments available at the accelerator control panel.

RESULTS

A. Damage Rate

The dependence of damage rate $d\rho/d\phi$, the resistivity increase per integrated electron flux, on incident electron energy E_i is given in Fig. 1 (solid curve). This plot is appropriate since the resistivity was observed to increase linearly with electron dose at each energy. Extrapolation of the curve in Fig. 1 to zero damage rate allows a determination of E_d, the minimum electron energy necessary to eject permanently a copper atom from its lattice site. It is more conventional to discuss the minimum threshold displacement energy T_0, the minimum energy which must be transferred to a copper atom to permanently eject it from its lattice site. The word permanent is used in an operational context, since

[8] A. Sosin and H. H. Neely, Rev. Sci. Instr. **32**, 922 (1961).
[9] R. L. Garwin, Rev. Sci. Instr. **29**, 223 (1958).

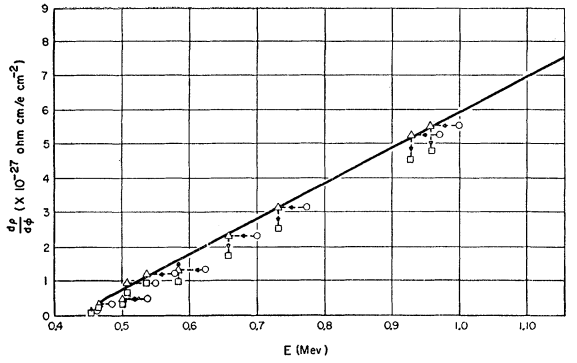

FIG. 2. The dependence of damage rate on electron energy. The encircled points are data points; for these points the abscissa represents incident electron energy. The points enclosed in triangles correspond to the encircled points as indicated, with a simple correction for electron energy degradation in the sample; for these points the abscissa represents the effective electron energy. The points enclosed in squares have been corrected further for electron straggling.

thermal activation will eventually allow any displaced atom to return to a corresponding lattice vacancy. Such recombination has never been observed by us during an experiment or following any reasonable holding period at 4.2°K. This is in accord with the observation of other observers (with the possible exception of the Oak Ridge investigators[5] following neutron irradiation). Recovery becomes measurable only when the sample temperature is raised to about 15°K.

Before discussing the implications of the damage-rate curve, Fig. 1, for radiation damage theory, a number of undesirable but concommitant features of the present investigation should be appraised.

(*1*) *Polycrystalline nature of the sample.* It has been implicitly assumed that all orientations of the lattice are equally presented to the electron beam. This assumption is reasonable since the angular scattering of bombarding electrons on traversing samples as thick as used here is very large. Moreover, the fact that our results appear to be in good general agreement with those of Corbett *et al.*[3] on samples with entirely different preparation also argues against significant preferred orientation effects.

(*2*) *Electron straggling.* The average path length S in the sample is greater than the thickness of the sample due to electron scattering. Lucasson and Walker[10] have discussed the correction which should be applied due to this effect, following the formalism of Yang.[11] Unfortunately, any attempt at a precise correction is precluded by uncertainties in the theory. Lucasson and Walker have proceeded by making a compromise in which the average increase in path length is assumed to be only $\frac{3}{4}$ of that calculated, following Yang. We have followed their method but derived a somewhat different expression for correction (see Appendix II). The correction is large, in terms of percentages, approximately 15% at 1 Mev and 50% at the lowest energies investigated. However, the absolute value of the correction, if applied to the data, does not affect the main features. Figure 2 shows the results of this correction.

(*3*) *Energy degradation of electrons.* A simple analysis, taking this correction into account, is given in Appendix I.

(*4*) *Boundary scattering.* Since the mean free path of electrons approaches the sample thickness at the temperature of measurement, a correction should be applied. The theory of Sondheimer[12] is applicable and has been applied to a similar situation by Corbett *et al.*[13] While the correction to the resistivity is appreciable, the correction to the increment of resistivity due to irradiation (about 1–2%) is within experimental uncertainty.

(*5*) *The lowest damage rate measured,* while low from the point of view of experimental feasibility, is still sensibly greater than zero.

We consider first the problem of arriving at the value of T_0. It is tempting to simply extrapolate the data of Fig. 1 to zero damage rate, using the standard expression[14] for copper,

$$T_m = 34.3E(1+E/1.022), \qquad (1)$$

where T_m, in units of ev, is the maximum energy which can be transmitted to an atom by an electron of energy E, in units of Mev. Such an extrapolation yields $T_0 = 22$ ev, corresponding to $E_d \simeq 450$ kev. However, this approach is incorrect. The error is due primarily to energy degradation, coupled with electron straggling.

According to the analysis in Appendix I, all data points corresponding to $E > E_d + 100$ kev should be corrected toward lower energy by approximately 45 kev to give an effective electron energy $\bar{E}$; when $E < E_d + 100$ kev, the correction is smaller and goes to zero for $E = E_d$. If E_d is set equal to 450 kev, the data points are shown in Fig. 2. The correction for electron straggling is also included. A notable feature of Fig. 2 is the character of the curve near 450 kev, particularly the two lowest-energy data points. The curve appears to approach the abscissa with increasing slope. The proper behavior of the curve at the lowest energies can only be predicted by a detailed theory, not yet available. Under rather simple, intuitively plausible assumptions, it can be shown that the slope of the damage rate curve should rise from its initial (not necessarily zero) value at threshold. If this is correct, the character of the Fig. 2

[10] P. Lucasson and R. M. Walker, Proc. Faraday Soc. (to be published).
[11] C. N. Yang, Phys. Rev. **84**, 599 (1951).
[12] E. H. Sondheimer, *Advances in Physics*, edited by N. F. Mott (Taylor and Francis, Ltd., London, 1952), Vol. I, p. 1.
[13] J. W. Corbett, J. H. Denney, M. D. Fiske, and R. M. Walker, Phys. Rev. **108**, 954 (1957).
[14] F. Seitz and J. S. Koehler, *Solid State Physics*, edited by F. Seitz and D. Turnbull (Academic Press Inc., New York, 1956), Vol. II, p. 328–331.

near threshold is due to an undercorrection in the lowest energy data points which, in turn, is due to assuming too high a value of E_d. Indeed, the analysis presented later indicates that T_0 is probably between 19 and 20 ev.

In order to attempt to fit the "damage-rate" curve of Fig. 1 or Fig. 2, we write,

$$\sigma_d(T_0,T_m)=\int_0^{T_m} P(T,T_0)\frac{d\sigma(T,T_m)}{dT}dT, \qquad (2)$$

where $d\sigma(T,T_m)$ is the differential cross section for transfer of energy T to an atom K by an electron capable of transferring a maximum energy T_m (in a head-on collision). P is a probability-of-ejection function; that is, if K receives an energy T, P is the probability that it will be permanently displaced from its lattice site. Walker and co-workers[10,13,15] have most thoroughly discussed various forms of P. The simplest assumption is that P is a constant, independent of the direction of the initial momentum of K. This gives rise to a "step-probability" function, P_1, where $P_1=0$ when $T<T_0$ and $P_1=1$ for $T\geq T_0$. Then Eq. (2) becomes

$$\sigma_d(T_0,T_m)=\int_{T_0}^{T_m}\frac{d\sigma(T,T_m)}{dT}dT. \qquad (3)$$

In a slight modification of this assumption, it has been suggested that it may be more appropriate to define a function P_2, where $P_2=0$ when $T<T_0$ and $P_2=b$, a constant less than unity, for $T\geq T_0$. The integral in Eq. (3) is then merely multiplied by this constant b. Although the introduction of such a constant appears trivial, and indeed is quite unimportant for events in the energy range presently investigated, the use of a "reduced step function" P_2, may significantly alter the prediction as to the number of displacements due to the high-energy transfers typical of heavy-particle irradiations.

The damage rate which results when one assumes that $P=P_1$ is also shown in Fig. 1, labeled "step." (In all curves of Fig. 1, we have taken $E_d=450$ kev. Although this is not correct, as discussed above, this curve is only slightly affected by this.) In plotting this curve, we have taken $\rho_F=1.5\times10^{-4}$ ohm cm/unit concentration of Frenkel pairs. This probability function is inadequate, even when modified to include a constant b. It should be noted, however, that the inability of a step function to account for the damage rate is most manifest in the energy range investigated here, near threshold. It may still be true that a step function is reasonably adequate for high-energy, heavy-particle irradiation if a factor b is included.

A step function appears to be a poor approximation to the correct form of P. Another approach followed by Walker and co-workers[13] is to introduce a "linear" function P_3 reasonably describing their observations. Here $P_3=0$ when $T<T_0-\Delta$, $P_3=1$ when $T>T_0+\Delta$, and P_3 increases linearly from zero to unity in the range $T-\Delta>T>T+\Delta$, becoming 0.5 at $T=T_0$. The energy Δ is somewhat adjustable. This probability function led to a value of $\rho_F=1.45\times10^{-4}$ ohm-cm/unit concentration, somewhat lower than the usually proposed value. Subsequently, Lucasson and Walker[13] extended their range of electron energy downward to 0.5 Mev. Using a linear function again, they concluded that $\rho_F=1.3\times10^{-4}$ ohm-cm/unit concentration, even lower than previously.

All of these approaches are quite empirical and none explicitly takes into account the crystallographic nature of the displacement process. Since the minimum energy to eject an atom from a lattice site should be a function of the direction as well as magnitude of the initial momentum of the struck atom K some account of this fact is necessary. The viewpoint adopted here is that it is sensible to talk about a threshold energy which has a rather sharp angular dependence and to note that in only one crystallographic direction in the lattice does this energy T_d take on a minimum value T_0. A theory based on these concepts is described later.

It should be noted, in passing, that the damage-rate curve is complicated by still another consideration. Several interstitial-vacancy configurations are produced by the irradiation. Each configuration may be expected to contribute differently to the resistivity. Since no evaluation of the importance of this effect is available, it will be assumed that all configurations contribute equally.

B. Recovery of Resistivity

In this section, we shall discuss the annealing of copper, primarily in stage I. It might appear to be necessary always to start an annealing study after irradiation at some chosen electron energy with the same amount of resistivity change. Due to the large variation in damage rates at the extremes of electron energies investigated, this was not readily practical. Since it is now established[3] that substages I_a, I_b, and I_c each obey first-order kinetics, it follows that there is no interaction between these substages or with subsequent recovery stages and that constant total damage is an unnecessary requirement in a study of these substages. The characteristics of substages I_d and I_e and the damage remaining beyond stage I are implicitly subject to a dose dependence; however, no particular effort has been made here to separate substages I_d and I_e. Interestingly, the results indicate somewhat surprisingly that the resistivity remaining after stage I has little energy dependence.

The main data on annealing are listed in Table I. Similar data due to other investigators are also included. Our data are the results of several individual experi-

[15] A. Lucasson, P. G. Lucasson, Y. Cusson, and R. M. Walker, International Conference on Properties of Reactor Materials and the Effects of Radiation Damage, Berkeley, England, Paper 23 (1961).

TABLE I. Percent resistivity recovery in stage I and in each substage of stage I.

	U. of I.[a]	U. of N. C.[b]	G. E.[c]	A. I.[d]	G. E.[c]	A. I.[d]	G. E.[c]	G. E.[c]	A. I.[d]	A. I.[d]	A. I.[d]
E (Mev)	10	2.0	1.40	0.97	0.93	0.77_5	0.69	0.65	0.58	0.48_5	0.46_2
T_m (ev)	1.2×10^6	206	115	64.9	61	46.5	40	37	31.2	24.6	23.0
I_a (%)	4	3.0	2.5	3.3	2.5	2.6	2.2	2.2	1.4	0.6	0
I_b (%)	8.5	12.0	13.1	12.8	12.6	13.6	13.3	13.4	14.6	15.9	17
I_c (%)	7.5	9.3	10.0	10.0	11.6	14.4	14.2	15.3	17.2	25.5	34
I_{a+b+c} (%)	20	24.3	25.6	26.1	26.7	30.6	29.7	30.9	33.2	42.0	51
I (%)	64		87.2	83[e]	87.3	84.7	87.9	88.5	85.7	85.9	85.9
ϕ[f]				63.4		60.7			162.5	192.3	139.5

[a] See reference 2.
[b] See reference 7.
[c] See reference 6.
[d] Present work.
[e] This value extrapolated from the resistivity at 55°K and the shape of the recovery curve (present recovery vs temperature) below 55°K.
[f] ϕ, the integrated electron flux, is in units of 10^{16} electrons/cm^2.

ments in each of which the samples had been annealed to 350°K in place, prior to irradiation, irradiated with electrons of a preselected energy, then annealed isochronally through stage I in five minute pulses. The initial 350°K anneal was not sufficient to completely erase the increase of the previous irradiation, but the amount of increase was always small (usually less than one percent of the radiation-induced increment). Tempering pulses were usually started at 25°K, then proceeded at a temperature interval ΔT, such that $\Delta T/T \approx 1/30$ through stage I.

Before discussing in detail the energy dependence of the relative substage magnitudes, some other pertinent observations will be mentioned. An irradiation was performed using electrons with an energy of 550 kev to an integrated flux of 1.48×10^{18} electrons/cm^2. Following the irradiation, isothermal recovery at 32.5°K of resistivity was monitored. The results were found to be in excellent agreement with the results of Corbett, Smith, and Walker.[3] That is, the kinetics were found to obey accurately first-order kinetics with a rate constant of 1.88×10^{-3} sec^{-1}. For comparison, Corbett *et al.* found a rate constant of 1.36×10^{-3} sec^{-1}. These values agree to approximately one percent in the temperature of measurement or activation energy governing the recovery, well within experimental error.

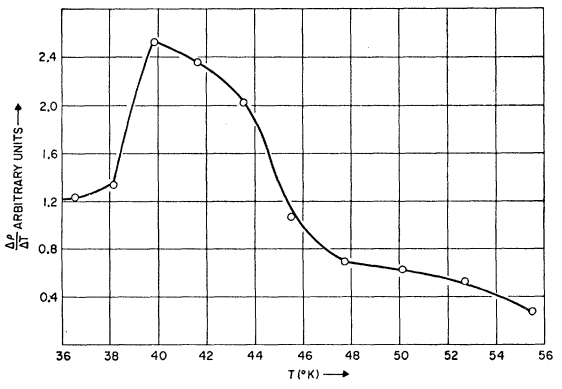

FIG. 3. The slope of an isochronal annealing curve in the Stage I_d—I_e temperature region. The incident electron energy was 550 kev.

The above result is not unexpected but emphasizes the truly monomolecular nature of recovery in substage I_c. Following this isothermal recovery study, the sample was annealed isochronally through the remainder of stage I. The results are shown in Fig. 3. The important point to note is that substages I_d and I_e are resolvable despite the fact that the incident electron energy is quite close to E_d. An implication of this result, based on the results of Corbett *et al.*[3] as well, is as follows: *Even near threshold, a substantial fraction of atom displacements result in interstitials that are displaced large distances from the site of ejection.*

This implication may be of assistance in the interpretation of the data in Table I as well. Consider, for example, the results that might have been anticipated for the energy dependence of substage magnitudes. Based on the reported activation energies for close pair recombination in substages I_a, I_b, and I_c, it is logical to assume that the interstitialcy that migrates in I_b is displaced further than that which migrates in I_a, etc. By a similar line of reasoning, one might expect that, as the energy of the incident electrons is reduced toward threshold, the relative magnitude of I_a would increase most rapidly, I_b next most rapidly, followed by I_c, etc. One would also expect that, below some energy, the stable damage should consist only of close pair configurations.

The data of Table I do not bear out this simple model. Since a calculation of displacement cross section presented later indicates that the ⟨110⟩ direction is particularly important for displacements near threshold, we consider a model in which the close pair configurations are disposed along a ⟨110⟩ direction from the site of the initial electron-atom collision. It seems logical in this model to retain the assumption that the interstitial-vacancy separation of the substage I_a configuration is less than the I_b configuration and this, in turn, is less than the I_c configuration. The problem is to understand why a more distant site, that peculiar to the I_c configuration, becomes relatively easier to reach as the electron energy is decreased than that of a closer configuration. Such a phenomenon, if real, must be due to a complex set of atomic interactions. For example, in

ejections along, or nearly along, a ⟨110⟩ direction, focusing action[16–19] may allow transport of an interstitial several lattice distances before relaxation effects set in which determine whether the interstitial atom will persist in its position or if a spontaneous recombination will eliminate this close pair configuration. If the ejection occurs at larger angles, defocussing is expected and the interstitial atom may be deposited at a closer site to the vacancy. However, recombination in the latter case may be prohibited due to the diverse motions of the atoms involved. This would result in an effectively higher threshold displacement energy for the I_a configuration than other configurations.

This model is quite speculative. It has its greatest merit in that it may explain the energy dependence of recovery in a reasonably simple fashion. The observed persistence of nonrecoverable resistivity beyond stage I near threshold energies may be explained in this way also. For, if the interstitials are displaced relatively long distances from a vacancy near threshold, trapping or other effects of impurities, dislocation, etc., will remain highly important.

There are other data which indicate the importance of long-range presumably ⟨110⟩ type ejections. The presence of a I_d-I_e separation, Fig. 3, can most easily be explained in this manner. Similarly, the internal friction results of Thompson[20] indicate the importance of long-range ejection, although the energy transfers involved in his neutron-irradiation experiment are admittedly much greater.

A consequence of this model is that all the reported close pair recovery stages are due to configurations disposed along ⟨110⟩ directions. Still another model is possible which preserves this assumption. Thus, it is conceivable that, while the relative magnitude of substage I_a has apparently gone to zero above threshold energy, in actuality the magnitude of substage I_a is nonzero in the range of energy investigated but appears to be zero because of limited sensitivity of measurement. If this were the case, one might, in principle, show that only substage I_a persists by decreasing the electron energy still further and irradiating for a very long time. This model seeks to circumvent the feature of the previous model in which a close pair created just above threshold takes on a configuration corresponding to substages I_b or I_c.

The two models proposed above appear to be in contradiction of the computer results of Vineyard and co-workers.[16] According to their results, the threshold displacement energies for ⟨110⟩ and ⟨100⟩ ejections are almost equal. This suggests a model in which the close pair configurations are established by ejection along ⟨110⟩ and ⟨100⟩ directions. Thus, the substage I_c configuration is reached along one of these directions, the ⟨110⟩, say, whereas the substages I_a and I_b configurations are reached along the ⟨100⟩ direction, characterized by a higher threshold energy for creation but lower recombination energies. Reasonable agreement with our experimental data, with the computer results of Vineyard and co-workers[16] and with the cross section calculation presented subsequently is affected by this model if it is further true that most displacements in the energy range investigated here are due to ⟨110⟩ ejection events—that is, that the relatively long-range displacements which result in substages I_d and I_e are due primarily to ejections along ⟨110⟩ directions. The difference between the I_a and I_b configurations probably is most easily explained by hypothesizing that both configurations represent an interstitialcy centered at the same position in the lattice but that the interstitialcy is formed by two atoms whose axes are oriented 90° apart in the two configurations.

Finally, there is a model in which each close pair configuration is reached along different directions—probably ⟨100⟩, ⟨110⟩, and ⟨111⟩. While the simplest in concept, this model is least likely to be correct since it would require that the threshold displacement energies in the three directions be almost equal. The results of Vineyard and co-workers,[16] for example, do not support such a conclusion.

There is a straightforward manner in which to test these models. This is to irradiate thin copper single crystals, oriented so that the electron beam penetrates one foil along a ⟨110⟩ direction and, in a second foil, along a ⟨100⟩ direction.

The possibility that directional effects may be important has been recognized by other investigators. In fact, Walker and co-workers[15] have performed electron irradiations of copper single-crystal whiskers oriented as suggested above. Their results do show a difference in the recovery characteristics for the two orientations. The difference is quite small; however, the whiskers had exceptionally large diameters, 0.005 in., for this experiment. A critical test should be performed with considerably thinner samples and at lower energies.

CALCULATED DISPLACEMENT CROSS SECTION

In the remainder of this paper, a theoretical calculation of the cross section for displacement of copper atoms by electrons is presented.

Consider a knock-on atom K which has just received kinetic energy T from a passing high-energy electron. As has been discussed previously,[21] there are three crystallographic directions which merit consideration as directions for easy ejection. These directions, indicated in Fig. 4, are ⟨100⟩, ⟨110⟩, and ⟨111⟩. In order for K to be ejected, it must pass through a configuration of

[16] J. B. Gibson, A. N. Goland, M. Milgram, and G. H. Vineyard, Phys. Rev. **120**, 1229 (1960).
[17] R. H. Silsbee, J. Appl. Phys. **28**, 1246 (1957).
[18] G. Liebfried, J. Appl. Phys. **30**, 1388 (1959).
[19] G. Liebfried and Chr. Lehmann, Z. Physik **162**, 203 (1961).
[20] D. O. Thompson, T. H. Blewitt, and T. K. Holmes, J. Appl. Phys. **28**, 742 (1957).
[21] A. Sosin, Materials in Nuclear Applications, A.S.T.M. Special Technical Publication No. 276, 1959 (unpublished).

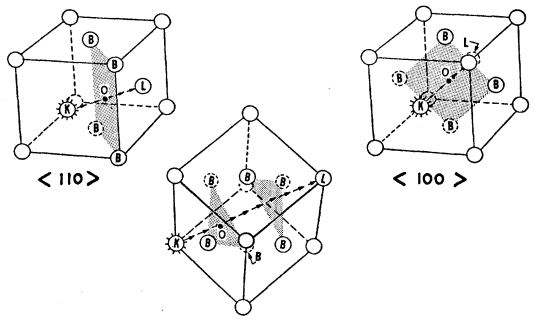

FIG. 4. Diagram to illustrate geometry of ejection processes in copper. The atom K is presumed to have received an impulse from a passing, high-energy electron and is initially projected in the three directions, as shown.

"barrier atoms" B in each case, imparting energy to these B atoms in so doing. The arrays are square, rectangular, and triangular, respectively, in the three cases being considered. The pertinent distances are shown in Fig. 4. and tabulated in Table II.

In a two-body collision approach, K then strikes another atom L in an essentially head-on manner after passing through an array of B atoms.

To evaluate these atomic collisions, it is necessary to choose some form of expression to represent the interaction between copper atoms. This problem has been discussed by a number of authors, most recently by Vineyard and co-workers.[16] We have used all three forms of Born-Mayer potential suggested by Vineyard and co-workers after the lead of Huntington and Seitz[22] and Huntington[23]:

$$V=A\exp(-\nu r), \tag{4}$$

where the parameters A and ν are given in Table III. For further discussion of Eq. (4), the reader is referred to Vineyard and co-workers.[16]

First, consider the mechanics of the collision process depicted in Fig. 5. In the spirit of the impulse approximation, we fix a barrier atom B at a distance b from the undeflected path of K. We assume a central force, $\mathbf{F}$, between K and B given by the gradient of a Born-Mayer type potential energy:

$$\mathbf{F}=-\nabla V=-\nabla\{A\exp(-\nu r)\}, \tag{5}$$

where r is the distance between K and B. The impulse

TABLE II. Atomic separation (see Fig. 4).

Direction	Number of B atoms	OB (Å)	$\frac{1}{2}KL$ (Å)
⟨100⟩	4	1.80	1.80
⟨110⟩	4	2.21	1.27
⟨111⟩	3	1.47	···

[22] H. B. Huntington and F. Seitz, Phys. Rev. **61**, 315 (1942).
[23] H. B. Huntington, Phys. Rev. **91**, 1092 (1953).

TABLE III. Constants in Born-Mayer potential after Vineyard and co-workers[a] [see Eq. (4)].

Potential	A (ev)	ν (Å^{-1})
1	9.4×10^5	6.65
2	2.3×10^4	5.10
3	3.5×10^3	4.05

[a] See reference 16.

transferred to B is

$$I=\int_{-\infty}^{+\infty}F_\perp dt=2\int_0^{\infty}F_\perp dt, \tag{6}$$

again under our simple assumption that B remains fixed in position. $F_\perp=|\mathbf{F}|\sin\theta=|\mathbf{F}|b/r$, is the transverse component of force. Equation (6) may be rewritten as

$$I=\nu A(2mb^2T^{-1})^{\frac{1}{2}}\int_b^{\infty}(r^2-b^2)^{\frac{1}{2}}\exp(-\nu r)dr, \tag{7}$$

using the kinetic energy expression, $dx=(2Tm^{-1})^{\frac{1}{2}}dt$.

The integral of Eq. (7) is the zeroth-order modified Bessel function of the second kind $K_0(b\nu)$. For large arguments $b\nu$ as encountered here, an excellent approximation[24] is $K_0(b\nu)=(\frac{1}{2}\pi b^{-1}\nu^{-1})^{\frac{1}{2}}\exp(-b\nu)$. The energy transferred to a B-type atom is $\epsilon=I^2/2m$. Thus we take as our working expression

$$\epsilon=\tfrac{1}{2}\pi b\nu(A^2/T)\exp(-2b\nu). \tag{8}$$

Once a value of T is assumed, ϵ can be evaluated for each set of Born-Mayer parameters and each of our three dominant crystallographic directions. The results of this evaluation are given in Table IV. We have listed T_1, which is 4ϵ, for the ⟨100⟩ and ⟨110⟩ directions, and 3ϵ for ⟨111⟩ direction. In making this evaluation, T has been set equal in turn to values between 17 and 22 ev. There is some inconsistency here since this should only apply for one of our crystallographic directions. However, since the exponential factor in Eq. (8) is the important term to be considered, the values in Table IV should be typical for any direction (with the use of the impulse approximation), but should only be truly applicable for one direction. Furthermore, the impulse approximation should be most valid when $\epsilon\ll T$. It is fortunate that this condition is best obeyed for the ⟨110⟩

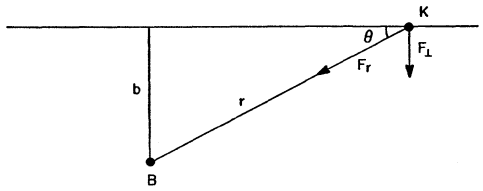

FIG. 5. Parameters entering into impulse approximation. The atom K is projected horizontally past a barrier atom B.

[24] G. N. Watson, *Theory of Bessel Functions* (Cambridge University Press, New York, 1948).

direction, since Eq. (8) will be used seriously for only this direction.

Several features should be noted. First, the values of T_1 for the ⟨111⟩ direction are not sensible since $T_1 > T_0$. Thus the impulse approximation fails completely here. Nevertheless, it is reasonable to deduce that T_1 is large for the ⟨111⟩ direction, indicating that ⟨111⟩ events may be ignored here. Now consider the values of T_1^{100} in Table IV. With the possible exception of the value derived using V_2, the values are again unreasonably high, and even the use of V_2 yields a value which is too high to be used subsequently with any confidence. Only the values of T_1^{110} are sufficiently small to be used with reasonable confidence. This is reinforced by other considerations as well. For example, the experimental results of Thompson, Holmes, and Blewitt,[20] Thompson,[25] Schmidt and Sharp,[26] and others indicate that the energy loss per atom distance traveled by an interstitialcy during bombardment is small. T_1^{110} is closely identified with this energy. Our values of T_1^{110} agree well with the computer results of Vineyard and co-workers.[16]

Thus far, attention has been restricted to ejections directly along the main crystallographic directions. Now consider the mechanics of collision when K initially makes an angle β with respect to the ⟨110⟩ direction. A precise calculation of the energy loss is formidable, since it requires that two angles be specified for each such event. Fortunately, our results do not require us to become involved in such complications. Instead, we shall make a single computation for the case where the initial velocity vector of K is projected at angle β off the ⟨110⟩ direction in the (001) plane (see Fig. 4) and use the resulting expression as a general one. Even this calculation is complicated by several factors which will be ignored:

(1) The direction of K's velocity vector may become more nearly parallel to the ⟨110⟩ direction as K approaches the barrier atom rectangle (assisted focusing). However, the effect of the K-L interaction will tend to have the reverse effect.

(2) The B atom will actually relax during and after the approach of K.

Bearing in mind these approximations, Eq. (8) is still valid for energy loss to each B atom when

$$b \rightarrow b \pm (1/\sqrt{3})a \tan\beta, \tag{9}$$

where the plus sign applies for two B atoms, the minus sign for the other two atoms. The derivation of Eq. (9) is an application of simple geometry. The distance, $a = 1.275$ Å, represents one-half the distance between K and L. Proceeding further, one derives the working expressions

$$4\epsilon = T_1 \cosh[(2/\sqrt{3})\nu a \tan\beta] \equiv T_1 \cosh(\mu \tan\beta). \tag{10}$$

The constant μ in the expression for 4ϵ is also given in Table IV.

Consider the mechanism of a head-on K-L collision. In a simple two-body, hard sphere approach, K imparts all its energy to L in such a collision. In a manner used by many investigators one defines a hard-sphere diameter,

$$D = \nu^{-1} \ln(2AT_2^{-1}), \tag{11}$$

where T_2 would represent a second contribution to the energy loss for the knock-on atom, to be added to T_1. It is possible to use this approach to estimate the threshold energy, T_0, if the value of D appropriate to the problem is inserted in Eq. (11). The entire calculation is quite crude and merely serves to indicate the relative magnitude of T_0 for different potentials in various directions. Instead of resorting to such estimates, we have adopted a threshold energy in the range of 17 to 22 ev and deduced the value of T_2 by subtraction: $T_2 = T_0 - T_1$.

Two more considerations must be made before writing down the displacement cross section for ⟨110⟩-type ejections. First, we assume that the directions of incidence of the high-energy electrons are entirely random with respect to all crystallographic directions. In this way, we may introduce an angle, δ, the angle between a ⟨110⟩ direction and the incident electron direction, and then average over all values of δ permitted by subsequent energy considerations.

Second, we must recognize that the energy imparted to K by an electron depends on the nature of the electron-atom interaction. The simplest manner to specify this nature is by the expression

$$T = T_m \cos^2\gamma, \tag{12}$$

where γ is the angle between the incident electron direction and the direction of the initial impulse given by the electron. Equation (12) is actually only approximately correct, but due to the large differences in the masses of electron and copper atom, the error is completely negligible.

We now write our primary expression

$$\sigma_d(T_0,T_m) = \frac{12}{4\pi}\int_0^{\delta_{\max}}\int_0^{T_m} 2\pi \sin\delta d\delta \, P(T,T_0,T_m,\delta)\frac{d\sigma(T,T_m)}{dT}dT. \tag{13}$$

TABLE IV. Tabulation of various parameters appearing in the calculation for each of the potentials, V, used. See text for further explanation.

	V_1	V_2	V_3
T_1^{110}[a] (ev)	0.612–0.791	0.272–0.352	0.516–0.668
T_1^{100}[a] (ev)	20–26	3.5–4.5	14.1–18.3
T_1^{111}[a] (ev)	1.9×10^3–2.5×10^3	80–104	36–46.5
$\mu = (2/\sqrt{3})\nu a$	9.78	7.50	5.96

[a] Highest values correspond to $T_0 = 22$ ev; lowest values to $T_0 = 17$ ev.

[25] M. W. Thompson, Phil. Mag. 4, 139 (1959).
[26] R. A. Schmitt and R. A. Sharp, Phys. Rev. Letters 1, 445 (1958).

TABLE V. Calculated displacement cross sections in Cu. The numbers corresponding to the potential, V, denote the particular potential used in the calculation (see Table IV). Both the calculated cross section σ, in barns, and the ratio of this cross section to the value at 1.0 Mev, are given. ρ_F, the Frenkel resistivity, is given in units of 10^{-4} ohm cm per unit concentration.

V	3		3		3		3		3		3	
T_0 (ev)	22		21		20		19		18		17	
T_1 (ev)	0.516		0.540		0.568		0.596		0.630		0.668	
μ	5.96		5.96		5.96		5.96		5.96		5.96	
E (Mev)	σ (b)	$\sigma/\sigma_{1.0}$	σ (b)	$\sigma/\sigma_{1.0}$	σ (b)	$\sigma/\sigma_{1.0}$	σ (b)	$\sigma/\sigma_{1.0}$	σ (b)	$\sigma/\sigma_{1.0}$	σ (b)	$\sigma/\sigma_{1.0}$
0.45	0.006	...	0.177	0.008	0.579	0.024	1.218	0.046	2.108	0.073	3.254	0.106
0.50	0.967	0.046	1.611	0.071	2.439	0.100	3.465	0.131	4.708	0.163	6.188	0.210
0.55	2.731	0.130	3.644	0.161	4.738	0.194	6.015	0.227	7.495	0.260	9.197	0.299
0.60	4.789	0.228	5.893	0.260	7.173	0.293	8.649	0.327	10.280	0.357	12.136	0.394
0.65	6.840	0.325	8.209	0.362	9.641	0.394	11.244	0.424	12.996	0.451	14.829	0.482
0.70	9.152	0.435	10.510	0.463	12.017	0.491	13.785	0.530	15.586	0.541	17.762	0.577
0.75	11.321	0.538	12.784	0.563	14.345	0.586	16.145	0.610	18.092	0.628	20.304	0.660
0.80	13.433	0.638	14.925	0.658	16.622	0.679	18.490	0.698	20.526	0.713	22.601	0.734
0.85	15.486	0.736	16.999	0.749	18.792	0.768	20.617	0.778	22.730	0.789	24.853	0.807
0.90	17.424	0.828	19.034	0.839	20.851	0.852	22.732	0.858	24.748	0.859	26.578	0.863
0.95	19.277	0.916	20.884	0.920	22.677	0.927	24.673	0.931	26.835	0.932	29.112	0.946
1.00	21.046	1	22.692	1	24.467	1	26.488	1	28.806	1	30.780	1
1.05	22.748	1.081	24.375	1.074	26.191	1.070	28.287	1.068	30.365	1.054	32.651	1.060
1.10	24.329	1.156	25.978	1.145	27.937	1.142	29.778	1.124	32.153	1.116	34.259	1.113
1.15	25.919	1.232	27.470	1.211	29.333	1.199	31.257	1.180	33.652	1.168	35.754	1.162
1.20	27.366	1.300	28.861	1.272	30.853	1.261	32.948	1.244	34.952	1.213	37.116	1.206
1.25	28.548	1.356	30.315	1.336	32.239	1.318	34.053	1.286	36.252	1.258	38.368	1.246
ρ_F	2.76		2.56		2.37		2.19		2.01		1.88	

V	3		3		3		2		2		1		1	
T_0 (ev)	21		19		17		22		19		22		19	
T_1 (ev)	0.540		0.596		0.668		0.272		0.315		0.612		0.709	
μ	6.70		6.70		6.70		5.70		7.50		9.78		9.78	
E (Mev)	σ (b)	$\sigma/\sigma_{1.0}$	σ (b)	$\sigma/\sigma_{1.0}$	σ (b)	$\sigma/\sigma_{1.0}$	σ (b)	$\sigma/\sigma_{1.0}$	σ (b)	$\sigma/\sigma_{1.0}$	σ (b)	$\sigma/\sigma_{1.0}$	σ (b)	$\sigma/\sigma_{1.0}$
0.45	0.155	0.008	1.048	0.046	2.768	0.105	0.007	...	1.218	0.050	0.003	...	0.540	0.043
0.50	1.392	0.071	2.966	0.131	5.263	0.199	0.959	0.050	3.350	0.139	0.449	0.045	1.536	0.124
0.55	3.137	0.101	5.143	0.227	7.843	0.296	2.621	0.138	5.720	0.237	1.255	0.125	2.687	0.216
0.60	5.071	0.260	7.390	0.326	10.354	0.392	4.525	0.238	8.123	0.336	2.198	0.219	3.889	0.313
0.65	7.071	0.362	9.632	0.424	12.640	0.478	6.400	0.336	10.469	0.433	3.167	0.316	5.070	0.408
0.70	9.022	0.462	11.780	0.519	15.125	0.572	8.480	0.445	12.749	0.528	4.251	0.425	6.269	0.505
0.75	10.990	0.563	13.839	0.610	17.283	0.653	10.423	0.547	14.902	0.617	5.292	0.528	7.403	0.596
0.80	12.819	0.657	15.900	0.700	19.324	0.731	12.301	0.646	16.966	0.702	6.290	0.628	8.500	0.685
0.85	14.615	0.749	17.717	0.780	21.314	0.806	14.126	0.742	18.893	0.782	7.273	0.726	9.482	0.764
0.90	16.384	0.840	19.482	0.858	22.726	0.859	15.853	0.832	20.853	0.863	8.241	0.823	10.608	0.854
0.95	17.982	0.922	21.149	0.932	25.041	0.947	17.485	0.918	22.467	0.930	9.150	0.914	11.463	0.923
1.00	19.513	1	22.703	1	26.542	1	19.046	1	24.168	1	10.014	1	12.417	1
1.05	21.019	1.077	24.305	1.070	27.911	1.055	20.548	1.079	25.710	1.064	10.851	1.084	13.280	1.069
1.10	22.462	1.151	25.561	1.126	29.310	1.108	21.984	1.154	27.005	1.117	11.637	1.162	13.979	1.126
1.15	23.770	1.218	26.875	1.184	30.566	1.156	23.350	1.226	28.519	1.180	12.429	1.241	14.972	1.206
1.20	24.992	1.281	28.428	1.252	31.729	1.199	24.565	1.290	29.750	1.231	13.144	1.313	15.691	1.264
1.25	26.134	1.339	29.345	1.293	32.790	1.240	25.623	1.345	30.825	1.275	13.644	1.362	16.358	1.317
ρ_F	2.97		2.55		2.19		3.05		2.40		5.79		4.67	

We shall refer to $P(T,T_0,T_m,\delta)$ in Eq. (13) simply as the probability-of-ejection function. The factor $d\sigma$ is the differential cross section for transfer of energy in the range $T \rightarrow T+dT$ by an electron capable of transferring a maximum energy, T_m. Equation (1) gives the expression relating T_m to the electron energy E; the standard expression for $d\sigma$ is given by Seitz and Koehler.[14] The factors of 12 and 4π enter since there are 12 possible $\langle 110 \rangle$ directions in 4π steradians. There is no problem of overlap since the cones of directions which enter are sufficiently small.

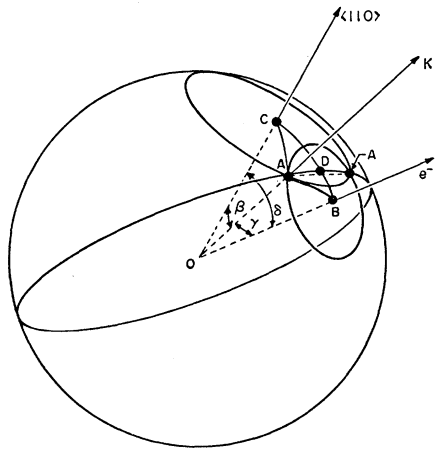

FIG. 6. Diagram to illustrate probability-of-ejection function used in calculation of displacement cross section.

Equation (13) may be integrated when $P(T,T_0,T_m,\delta)$ is specified. To derive this function, refer to Fig. 6. We have drawn a unit sphere with three vectors emerging from the center of the sphere. These vectors represent the direction labeled e^-, of the electron prior to collision with K, the direction labeled $\mathbf{K}$, of the atom immediately following the electron-atom collision, and a typical $\langle 110 \rangle$ direction. The angles β, γ, and δ are then

$$\beta = \angle(\mathbf{K},\langle 110\rangle), \quad \gamma = \angle(e^-,\mathbf{K}), \quad \delta = \angle(e^-,\langle 110\rangle) \quad (14)$$

as shown.

Rotating the $\mathbf{K}$ vector about the e^- vector traces out a circle on the sphere which is the locus of points where $T = T_m \cos^2\gamma$ is a constant [see Eq. (12)]; the circle on the sphere about the $\langle 110 \rangle$ vector is the locus of points where $T_1 \cosh(\mu \tan\beta) + T_2$ is constant [see Eq. (10)]. The overlap of two such circles is a measure of the probability of ejection. More precisely, the probability, P, is the fractional portion of the circumference of the circle traced out by $\mathbf{K}$ rotating about the e^- vector

which lies inside the circle about the ⟨110⟩ vector. This arc length is just twice the spherical angle ABC. Thus $P=2/\pi\angle ABC$, and, using spherical geometry

$$P=0, \quad \delta\geq\beta+\gamma;$$
$$P=(1/\pi)\arccos\{(\sin\delta\sin\gamma)^{-1}(\cos\beta-\cos\delta\cos\gamma)\}, \quad \beta-\gamma\leq\delta\leq\beta+\gamma; \tag{15}$$
$$P=1, \quad \delta\leq\beta-\gamma.$$

As written in Eq. (15), $P=P(\beta,\gamma,\delta)$. But β and γ are functions of T_0, T_m, and T, as given by Eqs. (10) and (12).

Our basic expression, Eq. (13), has been integrated on the IBM 709–7090 digital computers for a range of incident electron energies, 0.5 Mev $\leq E\leq$ 1.4 Mev. Some typical results of these calculations are given in Table V and Fig. 7.

The results in Table V are given directly in barns (10^{-24} cm^2); in addition, each set of cross sections has been normalized to the cross section at 1 Mev. An important point is immediately apparent on a normalized basis: there is little difference in any of the different sets of cross sections. Thus, to compare the calculations with experiment, any set may be chosen, providing an appropriate numerical factor is chosen to bring the experimental and theoretical data into coincidence at some point. This has been done in Fig. 8, with 1 Mev arbitrarily chosen as the "normalization point." A comparison of the circled data points in Fig. 8 with the calculated curves leads to an estimate of the threshold energy in copper: 19–20 ev.

Since the normalized cross sections are quite similar for the parameters investigated, the choice of most appropriate parameters must be based on the actual magnitude of the calculated cross section. To do this, we write

$$\sigma_d=(1/\rho_F)d\rho/d\phi, \tag{16}$$

where $d\rho/d\phi$ is the resistivity increase per unit electron flux and ρ_F is the Frenkel resistivity, the resistivity

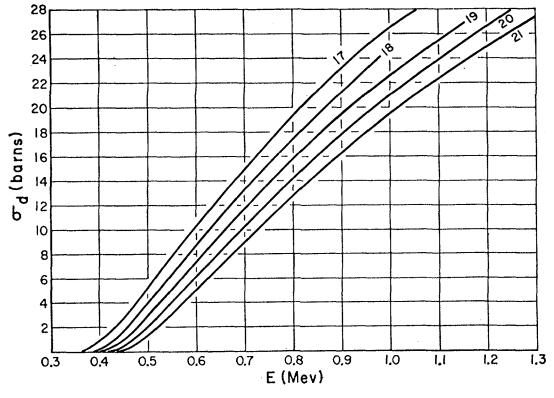

FIG. 7. Typical theoretical displacement cross section vs electron energy curves. The assumed threshold energies are indicated as 17–21 ev. The parameters used in this family of curves are those appropriate to V_3 with $\mu=6.70$ (see Table V).

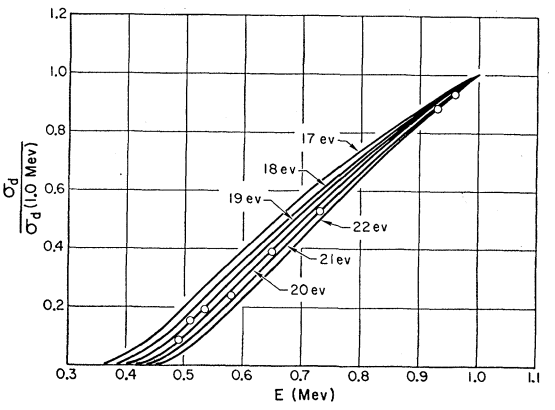

FIG. 8. The curve of Fig. 7 normalized to the displacement cross section at 1 Mev. These curves, while strictly applicable for a particular set of potential parameters, are only slightly changed by the other choices investigated. The circles indicate data points from the previous paper, corrected for electron energy degradation effects as described therein. Two lowest energy data points have been omitted since the energy corrections for these points require a knowledge of the threshold energy. These two points lie close to the 19-ev curve if a correction based on the assumption of a 19-ev threshold energy is made.

contribution due to unit concentration of interstitials and vacancies. Thus, ρ_F is the factor just used to normalize the cross-section calculations to the experimental data.

Unfortunately, the value of the Frenkel resistivity is still not well known in copper, despite the fact that there have been a number of calculations for both vacancies and interstitials. At this time, the best value must probably be derived from a comparison of resistivity and stored energy measurements following either electron or deuteron bombardment with the most reasonable theoretical results. It would appear, based on the experimental results of various workers[1–3,10,13,15,27–30] that 1.3×10^{-4} ohm cm $\leq\rho_F\leq3.6\times10^{-4}$ ohm cm. The present author would be inclined to select $\rho_F=3\times10^{-4}$ ohm cm as a preferred figure (all resistivities are for unit concentration of Frenkel defects).

The value of ρ_F necessary to bring the cross-section calculation into alignment with the observed $d\rho/d\phi$ value (at 1 Mev) are also given in Table V. It will be seen that V_1 should be rejected on this basis. This represents the "hardest" potential. The choice between the other two potentials is less clear but appears to favor V_3. V_3 represents a "softer" potential than commonly used. This is of particular importance in determining the character of the remainder of the ejection process wherein the interstitialcy is displaced some distance from the vacancy. It is significant, for instance, in determining whether the interstitialcy bears a two-body or crowdion behavior in its dynamic propagation away from the vacancy site, in determining the range

[27] R. W. Vook and C. A. Wert, Phys. Rev. **109**, 1529 (1958).
[28] A. Granato and T. Nilan, Phys. Rev. Letters **6**, 171 (1961).
[29] C. J. Meechan and A. Sosin, Phys. Rev. **113**, 422 (1958).
[30] A. Seeger and E. Mann, J. Phys. Chem. Solids **12**, 326 (1960).

of the interstitialcy, and in determining in what form the interstitialcy persists statically. A full discussion of these aspects is beyond the scope of the present report.

The displacement cross section σ_d just discussed has been evaluated under several approximations which require discussion. First, we have used several approximations involving β. The primary purpose in doing so is to yield a tractable expression to represent the angular dependence of T_d. The result of these approximations is to underestimate the angular dependence since the situation corresponding to easiest ejection of K through the barrier atoms B was adopted. This approximation is to a large extent compensated by a second approximation in which the impulse approximation is used throughout the calculation of barrier energy loss calculations. This second approximation overestimates the angular dependence of T_d since no account is taken of relaxation of B atoms nor the realignment of the velocity of K toward the ⟨110⟩ direction, both of which allow easier penetration of K through the B rectangle.

It would appear, therefore, that the main approximation that has been made in the calculation of σ_d comes from the neglect of displacements in other directions, specifically ⟨100⟩ directions. Yet, as we observe, the fit of the calculated cross section to the experimental curve leaves little to be desired, despite the fact that we have gone to values of T_m greater than $3T_0$. The agreement to such high energies may be fortuitous in that the contribution due to ⟨100⟩ ejections, presumably small in number, are sufficient to conceal a minor discrepancy between this theory and experiment.

The calculation described here is particularly concerned with the initial knock-on event and immediate atomic collisions. There is little to be said about subsequent collisions. It is, therefore, difficult to compare the results in this paper with related calculations of Leibfried[18,19] and Thompson and Nelson.[31] If there is a discrepancy between these, the present results, and these other investigators, including the experimental observations on the nature of sputtering,[31] it would appear to be in the distance of separation of interstitial and vacancy. That is, Thompson and Nelson explain their observations as an indication of the transfer of energy over long distance. Transport of mass (i.e., atoms) is believed to be limited. Whether or not this is truly a contradiction to our results is not established.

SUMMARY

It has been demonstrated that the minimum threshold displacement energy in copper is less than 22 ev. Furthermore, the dependence of recovery in the substages of stage I on the energy of the damaging electrons has been investigated. The close pair substages are found to increase in relative importance as the electron energy is reduced to threshold, as anticipated, but the manner in which the individual close pair substages depend on electron energy is more complex. Specifically, I_a decreases, I_b increases slowly, and I_c increases rapidly, respectively, as the electron energy is decreased to threshold.

The amount of damage which persists beyond stage I is found to depend only slightly on electron energy even quite close to threshold. In addition, stage I_e is found to exist for near-threshold bombardments. These observations indicate that atomic displacements are created near threshold in which the resulting interstitial atom is displaced a reasonably large distance from the site of the original electron-atom collision. This appears to indicate the importance of ejection events along directions near to ⟨110⟩ directions. Corroboration for this is found in a theoretical calculation of the displacement cross section which takes into account only such ejection events. Agreement with experiment is found if the threshold displacement energy is assumed to be 19 ev and the Frenkel resistivity to be between 2 and 3 μohm cm per atomic percent of interstitial-vacancy pairs.

ACKNOWLEDGMENT

It is a pleasure to acknowledge the vital experimental contributions of H. H. Neely. Discussions with J. A. Brinkman and critical manuscript reviews by F. H. Eisen and U. Gonser are also acknowledged. Discussions with U. Gonser and G. H. Vineyard, particularly on close pair recovery models, were most instructive.

APPENDIX I: CORRECTION FOR ENERGY DEGRADATION

We assume, for convenience, that the cross section for displacement σ_d is proportional to the difference in energy between the electron energy E and the (electron) displacement energy E_d.

The resistivity is observed to increase linearly with integrated flux ϕ. Thus the conductivity g initially decreases linearly with ϕ in a manner such as

$$g=g_0-\beta\phi(E-E_d), \tag{A1}$$

where g_0 is the pre-irradiation value of conductivity, $\phi(E-E_d)$ is proportional to σ_d, and β is a constant.

If G is the conductance and l the length of the cylindrical sample of radius r and cross-sectional area A,

$$lG=\iint_A gdA=g_0A-\beta\phi\iint_A (E-E_d)dA. \tag{A2}$$

We further assume that the energy of electrons decreases linearly from its value at incidence E_i to E at the depth p below the surface of the wire and that the electrons follow a straight line in transit through the wire, i.e., no straggling. The geometry of the problem is indicated in Fig. 9. If α is the energy loss per unit distance of electron traversal through the wire (approxi-

[31] M. W. Thompson and R. S. Nelson, Atomic Energy Research Establishment, Harwell, AERE-R3320, 1960 (unpublished).

mately 45 kev/0.001 in.),

$$E=E_i-\alpha p=E_i-\alpha[(r^2-x^2)^{\frac{1}{2}}-y]. \quad \text{(A3)}$$

We first consider the case where E_i is sufficiently greater than E_d so that the entire sample is damaged. Then Eq. (A2) becomes

$$lG=[g_0-\beta\phi(E_i-E_d)]A+\alpha\beta\phi\int_{-r}^{+r}dx\int_{-\bar{y}}^{\bar{y}}(\bar{y}-y)dy, \quad \text{(A4)}$$

where $\bar{y}\equiv(r^2-x^2)^{\frac{1}{2}}$.

Integration of Eq. (A4) yields

$$\bar{g}=g_0-\beta\phi\{[E_i-(8/3\pi)\alpha r]-E_d\}, \quad \text{(A5)}$$

where $\bar{g}$ is the average conductivity of the wire.

Thus the effective energy $\bar{E}$ is

$$\bar{E}=E_i-(8/3\pi)\alpha r. \quad \text{(A6)}$$

We now consider the case where E_i is sufficiently large so that there exists a boundary inside the cross section of the sample given by an expression,

$$E_d=E_i-\alpha\bar{p}, \quad \text{(A7)}$$

defining $\bar{p}$. In this case, we divide the cross section of the sample into a damaged area DA, and an undamaged area UA. Then

$$lG=\iint_{\text{DA}}[g_0-\beta\phi(E-E_d)]dA+\iint_{\text{UA}}g_0dA. \quad \text{(A8)}$$

It is further necessary to divide DA into two areas, numbered 1 and 2 in Fig. 9. Then Eq. (A8) becomes

$$\begin{aligned}lG=&g_0A-2\beta\phi(E_i-E_d)\int_u^r dx\int_{-\bar{y}}^{\bar{y}}dy\\&+2\alpha\beta\phi\int_u^r dx\int_{-\bar{y}}^{\bar{y}}(\bar{y}-y)dy\\&-2\beta\phi(E_i-E_d)\int_0^u dx\int_{\bar{y}-\bar{p}}^{\bar{y}}dy\\&+2\alpha\beta\phi\int_0^u dx\int_{\bar{y}-\bar{p}}^{\bar{y}}(\bar{y}-y)dy, \quad \text{(A9)}\end{aligned}$$

where $u\equiv[r^2-\frac{1}{4}(\bar{p})^2]^{\frac{1}{2}}$.

Proceeding as before, we arrive at an effective energy,

$$\begin{aligned}\bar{E}=&(E_i-E_d)\left[1-\frac{2}{\pi}\sin^{-1}\left(\frac{u}{r}\right)\right]\\&-\frac{\alpha r}{\pi}\left[\frac{8}{3}-4\left(\frac{u}{r}\right)+\frac{4}{3}\left(\frac{u}{r}\right)^3\right]+E_d. \quad \text{(A10)}\end{aligned}$$

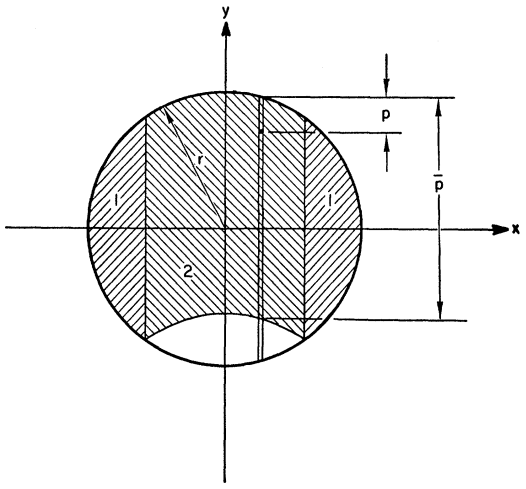

FIG. 9. A diagram for the evaluation of electron energy degradation.

Equation (A10) reduces to Eq. (A6) in the limit of $u\to 0$. Furthermore, $\bar{E}\to 0$ as $u\to r$. Finally, in the limit of small $\Delta E\equiv(E_i-E_d)$, the average conductivity becomes

$$\bar{g}=g_0-(\beta\phi/\pi\alpha r)(\Delta E)^2. \quad \text{(A11)}$$

APPENDIX II

According to Yang,[11] the average path length of the sample on traversing a distance y into the sample, parallel to the direction of incidence is

$$\lambda=y+ay^2, \quad \text{(A12)}$$

with

$$a=S/t^2=(\omega^2\chi_0)^{-1}, \quad \text{(A13)}$$

where S is the average incremental path length on traversing a foil of thickness t, χ_0 is a "radiation length" characteristic of the material (13.3 g/cm² for copper), and ω is a function of the electron energy, assumed to remain constant on passing through the foil. This increase in path length leads to an effectively increased flux, $\bar{\phi}$,

$$\bar{\phi}=\phi d\lambda/d\chi, \quad \text{(A14)}$$

where ϕ is the actual flux.

The resistivity in a uniform foil is

$$\rho(x)=\rho_0+\sigma_d\phi\rho_f=[g(x)]^{-1}, \quad \text{(A15)}$$

where ρ_0 is the resistivity prior to irradiation and $g(x)$ is the conductivity.

Then, for a uniform foil of thickness t

$$\bar{g}=\frac{1}{t}\int_0^t g(x)dx=2aKt\ln\left[1+\left(\frac{2aKt}{\rho_0+K}\right)\right], \quad \text{(A16)}$$

where $K\equiv\sigma\phi\rho_f$.

To proceed further, we approximate:

$$\bar{g}=\frac{1}{\rho_0+K}-\frac{aK}{(\rho_0+K)^2}t. \quad \text{(A17)}$$

For a wire sample, we integrate again, using Eq. (A17):

$$\bar{g}=\frac{1}{2r}\int_{-r}^{r}\left\{\frac{1}{\rho_0+K}-2\frac{aK}{(\rho_0+K)^2}(r^2-x^2)\right\}dx, \quad \text{(A18)}$$

$$\bar{g}=\frac{1}{\rho_0+K}-\frac{\pi}{4}\frac{aK}{(\rho_0+K)^2}d. \quad \text{(A19)}$$

The correction to the resistivity increase due to irradiation is, approximately,

$$\Delta\rho_c=\tfrac{1}{4}\pi aKd.$$

Since K is the true increase in resistivity, the desired increase in resistivity to compare with theory is

$$\rho=\rho_m(1+\tfrac{1}{4}\pi ad)^{-1},$$

where ρ_m is the measured resistivity increase.

PHYSICAL REVIEW VOLUME 126, NUMBER 5 JUNE 1, 1962

Far Infrared Dielectric Dispersion in $BaTiO_3$, $SrTiO_3$, and TiO_2

W. G. Spitzer, Robert C. Miller, D. A. Kleinman, and L. E. Howarth
Bell Telephone Laboratories, Murray Hill, New Jersey

(Received January 24, 1962)

The room temperature reflectivity of $BaTiO_3$, $SrTiO_3$, and TiO_2 has been measured from 5000 to 70 cm^{-1}. These data have been analyzed by the Kramers-Kronig method and by classical dispersion theory. All of the infrared-active fundamental vibrations allowed by crystal symmetry have been measured and characterized by their dispersion parameters. Of particular interest is the low-frequency mode which recent theories show is responsible for ferroelectricity in $BaTiO_3$ and $SrTiO_3$ and is found at 33.8 and 87.7 cm^{-1}, respectively. The unusually large damping found for this mode can explain the observed microwave loss tangents. The strength of the mode accounts for the large values of the low-frequency dielectric constant. This mode, as well as the highest frequency mode, 510 and 546 cm^{-1} in $BaTiO_3$ and $SrTiO_3$, respectively, is associated with TiO_6 octahedra vibrations. A previously unreported mode at 183 and 178 cm^{-1} for $BaTiO_3$ and $SrTiO_3$, respectively, has also been found and assigned to a cation-(TiO_3) vibration. In rutile, three resonances are observed for the ordinary ray and one for the extraordinary ray, as required by theory. As with the titanates, the high dielectric constant is associated with the low-frequency mode. An analysis of the strengths of all of the resonances shows that they involve reasonable effective charges for ionic crystals.

INTRODUCTION

ONE of the most striking characteristics of the oxide ferroelectric materials,[1] such as the titanates and niobates, is the large value of ϵ_0 the dielectric constant in the microwave and lower-frequency parts of the electromagnetic spectrum. At temperatures in the neighborhood of the Curie point of these materials, dielectric constants of the order of 10^4 are observed. In contrast to these large values, the high frequency or optical dielectric constants ϵ_∞ are below 10. These materials have not in most cases been studied in the portion of the frequency spectrum, called the *transition region*, where the dielectric constant changes from ϵ_∞ to ϵ_0. Considered in the present paper are two materials which in some temperature region are ferroelectric, $BaTiO_3$ and $SrTiO_3$. Rutile,[2] TiO_2, which is not ferroelectric but exhibits high values for ϵ_0 and has the TiO_6 octahedra structure in common with the titanates, was also studied. At room temperature, where these materials are investigated, $BaTiO_3$ is tetragonal and ferroelectric, $SrTiO_3$ is cubic and paraelectric, and TiO_2 is tetragonal and a normal dielectric.

On the microwave side of the transition region, the two highest frequencies at which single crystals of $BaTiO_3$ have been measured, 0.8 cm^{-1} (24 kMc/sec)[3] and 1.87 cm^{-1} (56 kMc/sec),[4] both indicated a room temperature dielectric constant for electric fields perpendicular to the optic axis ϵ_{11} of 2000. (For convenience, all frequencies will be given in cm^{-1}.) The loss tangent was reported to be about 0.1. Measurements on single-crystal $SrTiO_3$ at frequencies up to 1.2 cm^{-1} (36 kMc/sec)[5] did not show any dispersion in the dielectric constant ϵ which is[6] about 310 at room temperature. The loss tangent at room temperature is 1.5×10^{-3} at 0.73 cm^{-1} (22 kMc/sec).[5]

Both $SrTiO_3$ and $BaTiO_3$ have been studied by Last[7] from 1000 cm^{-1} to about 300 cm^{-1}. Last claimed to have observed two of the three predicted optically active normal modes. The two resonances reported were as-

[1] For a general review on the subject of ferroelectricity the reader is referred to W. Känzig, in *Solid-State Physics*, edited by F. Seitz and D. Turnbull (Academic Press Inc., New York, 1957), Vol. IV.

[2] For a general review article on TiO_2, the reader is referred to F. A. Grant, Revs. Modern Phys. **31**, 646 (1959).

[3] T. S. Benedict and J. L. Durand, Phys. Rev. **109**, 1091 (1958).

[4] R. F. Trambarulo (quoted in reference 3).

[5] G. Rupprecht, R. O. Bell, and B. D. Silverman, Phys. Rev. **123**, 97 (1961).

[6] A. Linz, Jr., Phys. Rev. **91**, 753 (1953); G. Rupprecht (unpublished data).

[7] J. T. Last, Phys. Rev. **105**, 1740 (1957).